Data-centric Sensitivity Analysis of Quantum Kernels for Industrial Time Series

Kauã Dalla Riva Cucco Barbosa[1], Everson da Silva Flores[1], Bruna de Vargas Guterres[2], Silvia Silva da Costa Botelho[1] and Marcelo Rita Pias[1]

***Abstract*— A factorial sensitivity analysis of quantum and classical kernel behavior is presented for industrial anomaly detection under constrained representational conditions. Support Vector Machines with an RBF kernel and a Quantum Support Vector Machine with a quantum inversion test (qIT) kernel are evaluated on an industrial benchmark dataset. Encoding resolution $Q \in \{2, 4, 6, 8\}$ and training volume $n \in \{60, 120, 240\}$ are treated as explicit experimental variables within a data-centric quantum machine learning framework. Two industrial scenarios with different anomaly ratios are analyzed under identical preprocessing conditions. The results suggest that kernel behavior varies with encoding resolution and training volume in both scenarios. Different response profiles were observed for the RBF and qIT kernels under representational compression. More stable transitions across neighboring factorial configurations were produced by the qIT kernel. The factorial responses further suggest that encoding resolution works as an experimental design variable within industrial quantum machine learning workflows.**

***Keywords*— Quantum machine learning, quantum support vector machine, data-centric QML, industrial anomaly detection, representational compression and factorial sensitivity analysis.**

I. Introduction

Industrial cyber-physical systems require anomaly detection methods capable of identifying subtle deviations in multivariate sensor behavior [1], [2]. In manufacturing environments, incipient faults do not normally appear as isolated signal spikes. Gradual changes are instead observed in the data correlation structure among interconnected sensors. Fault isolation becomes difficult under low data conditions. This difficulty increases when labeled anomalies are not sufficiently available [3], [4].

Classical machine learning approaches are still commonly used for industrial fault detection. Supervised methods depend on reliable labels. Performance may be affected by class imbalance. Unsupervised reconstruction models are sensitive to noise and drift [4]. Threshold selection in this case also affects detection stability. These limitations motivate the investigation of alternative representation mechanisms.

Quantum Machine Learning (QML) has been investigated as an alternative computational paradigm [2], [5], [6]. Classical data are mapped into high-dimensional Hilbert spaces through quantum feature embeddings. Kernel-based quantum models have therefore been evaluated for industrial anomaly detection. Most studies report predictive performance under fixed preprocessing configurations. The sensitivity of kernel behavior to representational compression remains insufficiently explored. Encoding resolution is commonly treated as a static implementation parameter. Training volume is also usually fixed in the evaluation step [5].

The data-centric quantum machine learning (*dc-qml*) framework treats representation and encoding decisions as experimental design variables [7]. Under this framework, kernel behavior may vary with the structure of the encoded representation. The amount of training data may also influence kernel similarity estimation. The interaction between these design variables remains insufficiently characterized in industrial anomaly-detection scenarios.

Recent studies on quantum kernels and QSVM-based anomaly detection have explored applications in critical infrastructure, industrial cybersecurity, wind turbine monitoring and medical classification. Improvements in AUC and F1-Score were reported in comparison with classical approaches [2], [8], [9]. However, limitations related to noise sensitivity and hardware degradation are recurrent issues [3], [4]. These studies also address quantization, feature compression, encoding resolution, and training window configuration from a *dc-qml* perspective. The *contribution of this work* is the adoption of a *dc-qml* design framework to evaluate how quantization levels and training windows affect quantum and classical kernel behavior in industrial anomaly detection.

This paper presents a factorial sensitivity analysis of quantum and classical kernel behavior under controlled representational constraints. A classical Support Vector Machine with RBF kernel is evaluated against a Quantum Support Vector Machine with quantum inversion test (qIT) kernel. The SKAB industrial benchmark dataset is used as the experimental basis. Two industrial scenarios with different anomaly ratios are evaluated under identical preprocessing conditions.

The training volume is varied according to $n \in \{60, 120, 240\}$. The encoding resolution is varied according to $Q \in \{2, 4, 6, 8\}$. Both variables are evaluated independently within a controlled factorial protocol.

The following research questions are addressed in this paper:

RQ1: How does encoding resolution influence the stability of quantum and classical kernel anomaly detection under constrained training regimes?

RQ2: How does the interaction between training volume and encoding resolution affect error distribution across industrial anomaly scenarios?

Performance in anomaly detection is commonly evaluated using the F1 Score, False Alarm Rate (FAR), and Missed Alarm Rate (MAR). The F1 score balances detection sensitivity and prediction precision under imbalanced conditions. FAR

[1]Computer Science Center, Federal University of Rio Grande (FURG), Rio Grande, Brazil. [2]Postgraduate Program on Robotics and Artificial Intelligence, Technological University of Uruguay (UTEC), Rivera, Uruguay.

quantifies false positive detections during nominal operation. MAR measures the proportion of undetected anomalies during inference. The analysis focuses on the interaction between encoding resolution and kernel response under low data industrial conditions. Variations in encoding resolution may alter the induced similarity structure. Changes in training volume may also affect the formation of kernel boundaries during classification. The remainder of this paper presents the dc-qml framework, methodology, results and conclusions.

II. Data-Centric QML design: models and data

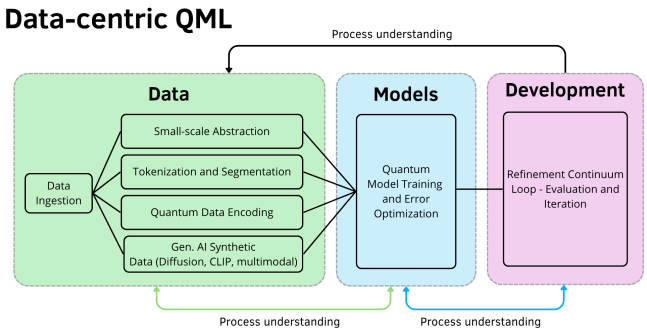

Fig. 1. Components of the data-centric QML framework (*dc-qml*) [7].

Under the *dc-qml* framework [7], variations in representation may change kernel similarity estimation during classification. The present work instantiates two variables from the *dc-qml* design approach. The encoding resolution (i.e., quantization level) Q controls the feature-encoding resolution prior to quantum state preparation. Lower Q values lead to coarser representations through increased representational compression. Higher Q values preserve finer variations in the encoded feature space. The training volume (i.e., window size) n controls the amount of nominal sample data available for kernel estimation.

Both variables are treated as explicit factors in a factorial experimental protocol. Fig. 1 summarizes the evaluation and refinement structure adopted in this work. The framework integrates representation preparation, encoding, model evaluation and iterative refinement within a unified workflow.

Current NISQ hardware creates constraints on qubit count and coherence limits [10], [11]. The behavior of QSVM models has also been shown to vary under different data partitioning strategies [9], [12]–[14]. Q and n are therefore treated as experimental variables rather than fixed implementation parameters.

Table I summarizes the *dc-qml* workflow components [7]. This work instantiates two components of that structure: Small-Scale Abstraction through the encoding resolution Q, and Data Ingestion through the training window size n. Both variables are evaluated under controlled factorial conditions in Section III.

III. Methodology

A. Dataset and Scenario Construction

The SKAB benchmark was used as the experimental dataset [15]. It represents an industrial water circulation system instrumented with a set of sensors as follows: two accelerometers, a pressure transducer, a thermocouple, a voltmeter, an ammeter and a flow meter. Sensor signals were sampled and recorded at one-second intervals under controlled conditions with injected fault events.

The dataset was chosen because it contains gradual transitions between nominal and anomalous behavior. Such transitions are suitable for the evaluation of representational sensitivity under constrained industrial conditions. The multivariate structure of the sensor dataset also allows the analysis of kernel behavior as a function of encoding resolution Q and training volume n.

Two scenarios from the SKAB "others" collection were selected for evaluation. Both scenarios originate from the same physical installation. However, the data show different anomaly ratios and fault-onset timings. Scenario A comprises 745 samples with fault onset at sample index 557. Scenario B contains 1137 samples with fault onset at sample index 568. Both scenarios simulate fluid disturbances in the water circulation system, corresponding to injected fault events of fluid leaks and fluid additions.

The test window size was fixed at 60 samples for both scenarios. Scenario A has 45 nominal samples and 15 anomalous samples within the test window, which corresponds to an anomaly ratio of 25%. Scenario B includes 39 nominal samples and 21 anomalous samples, which corresponds to an anomaly ratio of 35%. Figs. 2 and 3 present the training and test partitions used in this work.

Training volume at windows of $n \in \{60, 120, 240\}$ samples were extracted immediately before each fault onset. Only nominal samples were included in the training partitions. The resulting protocol isolates the interaction between training volume and encoding resolution under controlled anomaly conditions.

B. Quantum Circuit Implementation

Quantum method implementation and execution used `AerSimulator` from `qiskit-aer` (Qiskit 1.x). No physical quantum native device was used and results are therefore free from gate errors, decoherence and crosstalk noise.

Preprocessing followed the pipeline described in Section III. Data encoding was carried out using a parameterized feature map. Each layer applied Hadamard gates, followed by single-qubit $R_z(x_i)$ rotations and pairwise $R_{zz}(x_i \cdot x_j)$ interactions. Three re-upload repetitions produced a six-layer circuit across Q qubits.

Kernel similarity was estimated via the qIT, with $n_{\text{shots}} = 1000$. The resulting matrix was used as a precomputed kernel in the OC-SVM solver, with $\nu = 0.1$. Matrix symmetrization and regularization were applied to stabilize optimization prior to classification.

C. Experimental Protocol

Both kernel-based models (RBF and qIT) operate under a one-class unsupervised setting [13], in which the decision boundary is estimated using nominal training samples only, without any anomaly labels. A controlled factorial protocol

TABLE I

COMPONENTS OF A DATA-CENTRIC QUANTUM MACHINE LEARNING (*dc-qml*) WORKFLOW AND THEIR RELATION TO FACTORIAL KERNEL EVALUATION.

Component	**Workflow Function**	**Associated Methods and Techniques**
Data Ingestion	Industrial sensor data are prepared and organized for model training and evaluation.	Normalization, standardization, window extraction, anomaly labeling and preprocessing validation.
Small Scale Abstraction	The original sensor data space is reduced to a compact set of latent representations prior to encoding.	PCA, dimensionality reduction, feature compression and latent representation mapping.
Tokenization and Segmentation	Temporal data samples are partitioned into structured inputs for controlled encoding.	Fixed window segmentation, encoding resolutions (quantization levels) and token-based representations.
Quantum Data Encoding	Classical representations are mapped into Hilbert space through quantum feature embedding.	IQP feature maps, quantum feature maps and qubit-based encoding.
Quantum State Preparation	Quantum states are initialized for kernel estimation.	Parameterized quantum circuits, qubit initialization and state vector simulation.
Tensor Network Compression	Computational complexity is reduced in high-dimensional quantum representations.	MPS, SVD, tensor contraction and truncated decomposition methods.
Synthetic Data Generation	Training data distributions are expanded through artificial sample generation.	QGANs, diffusion models and hybrid-classical quantum generation pipelines.
Quantum Model Training	Quantum and classical kernel models are trained under identical preprocessing conditions.	QSVM, RBF SVM, qIT kernels, and kernel-based classification.
Evaluation and Refinement	Evaluate factorial behavior across encoding dimensions and training volume configurations.	F1 Score, FAR, MAR, ablation analysis and encoding refinement.

was defined over two independent variables: training volume $n \in \{60, 120, 240\}$ and encoding resolution $Q \in \{2, 4, 6, 8\}$. The latter controls the amount of representational detail (as quantization levels) preserved prior to quantum state preparation. Lower Q values lead to coarser representational compression. Higher Q values preserve finer variations in the encoded feature space. Each factorial configuration was repeated 15 times using different random seeds. The results were averaged across all repetitions and variability statistics were calculated.

Both the classical Support Vector Machine with RBF kernel and the Quantum Support Vector Machine with qIT kernel [13], [14] were evaluated under identical preprocessing conditions. The data were standardized using a `StandardScaler` fitted only on the training data partitions. Principal Component Analysis (PCA) reduced the original eight sensor channels to Q principal components, each mapped directly to one qubit, where $Q \in \{2, 4, 6, 8\}$ defines the encoding resolution evaluated in the factorial protocol.

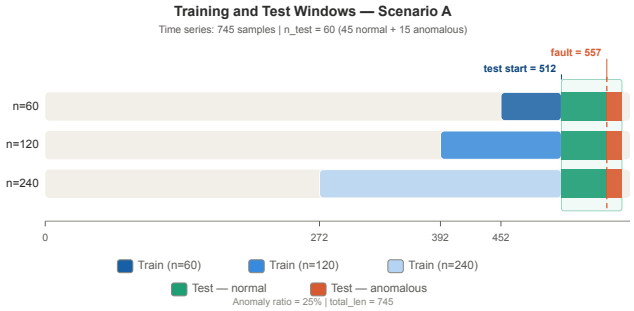

Fig. 2. Training and test window partitions for Scenario A. Fault onset occurs at index 557. The test window contains 15 anomalous samples out of 60 test samples.

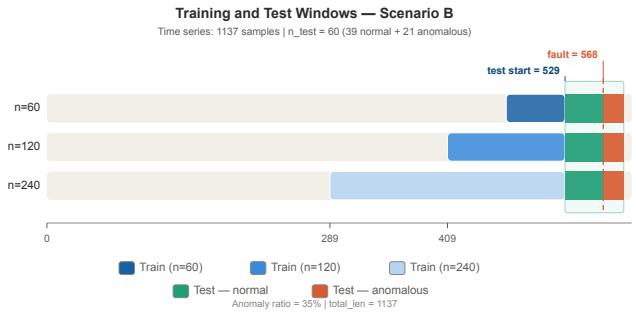

Fig. 3. Training and test window partitions for Scenario B. Fault onset occurs at index 568. The test window contains 21 anomalous samples out of 60 test samples (anomaly ratio of 35%).

D. Performance Metrics

Performance was evaluated using the F1 Score, False Alarm Rate (FAR) and Missed Alarm Rate (MAR). Let TP, FP, TN and FN be true positives, false positives, true negatives and false negatives, respectively. FAR is defined as $FAR = \frac{FP}{FP+TN}$ and quantifies false positive detections during nominal operation. MAR is defined as $MAR = \frac{FN}{TP+FN}$ and measures the proportion of anomalous samples incorrectly classified as nominal.

The evaluation focuses on the interaction between encoding resolution and kernel response under constrained industrial conditions. Variations in encoding resolution may change the induced similarity structure. Changes in training volume may also affect kernel boundaries during classification.

IV. RESULTS AND DISCUSSION

The experimental validation examines how the encoding resolution Q and training volume n influence kernel responses under controlled representational compression. Both scenarios simulate fluid disturbances in the same water circulation system, corresponding to injected fault events of fluid leaks and

fluid additions: Scenario A (`other/1.csv`, 745 samples, anomaly ratio of 25%) and Scenario B (`other/3.csv`, 1137 samples, anomaly ratio of 35%). Factorial response curves over the (Q, n) configuration grid are analyzed for (i) a classical RBF kernel and (ii) a qIT kernel.

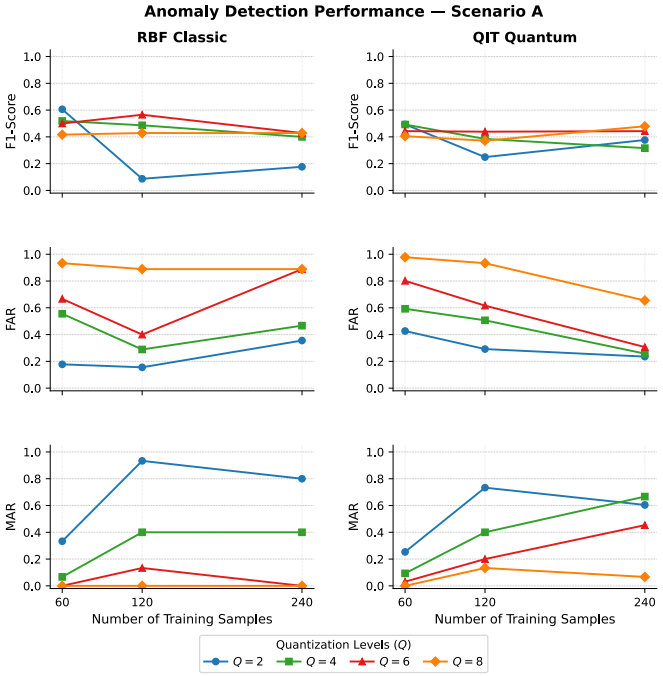

Fig. 4. Anomaly detection performance for Scenario A across training sizes ($n \in \{60, 120, 240\}$) and encoding resolutions ($Q \in \{2, 4, 6, 8\}$). F1-Score (top), FAR (middle) and MAR (bottom) are shown for classical RBF SVM (left) and QSVM with qIT kernel (right). Results are averaged over fifteen random seeds.

Figs. 4 and 5 show the factorial response curves for Scenarios A and B. F1 Score, FAR, and MAR are evaluated independently as functions of encoding resolution and training volume. Different response profiles are observed for both RBF and qIT kernels under representational compression.

In Scenario A (see Fig. 4), larger fluctuations are observed in the FAR and F1 Score results of the RBF kernel as the encoding resolution Q increases. This behavior becomes clearer at $Q = 8$, where FAR values remain high across all training windows. Under reduced representational compression, finer local variations remain preserved during kernel estimation. These variations may increase boundary instability under constrained training conditions. The qIT kernel produces smoother transitions across neighboring factorial configurations. However, reductions in FAR are associated with increases in MAR at larger training windows. This interaction suggests that error distribution varies with the balance between the encoding resolution and the number of available training samples.

A different response profile is observed in Scenario B (see Fig. 5) due to the higher anomaly ratio. Under this condition, the highest F1 Score values are obtained at $Q = 4$ and $n = 60$ for both kernels. Larger training windows do not systematically improve detection behavior. Broader nominal windows may include additional variability in the similarity structure used during kernel estimation. Under these conditions, local transition regions between nominal and anomalous states may become less separable. The factorial response curves therefore indicate that kernel behavior depends on the combined effect of encoding resolution, training volume and anomaly composition.

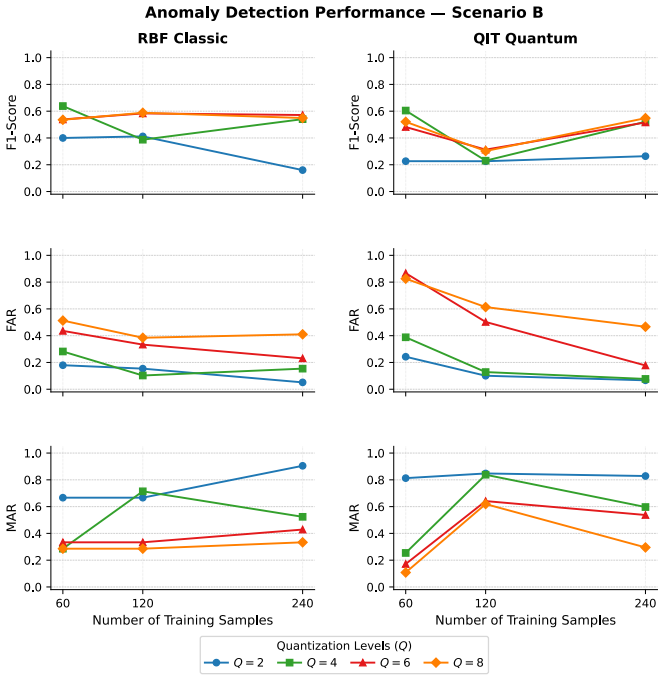

Fig. 5. Anomaly detection performance for Scenario B across training sizes and encoding resolutions at different encoding resolutions (quantization levels). The layout is identical to Fig. 4. The anomaly ratio differed (35% vs. 25% in Scenario A), which affects the F1-Score response across factorial configurations.

RQ1 — Effect of Q on kernel behavior. Distinct performance profiles are observed across the factorial configurations in Table II, and F1-Score does not increase monotonically with Q for either kernel. At $Q = 2$ in Scenario A, RBF F1 drops from 0.606 at $n = 60$ to 0.087 at $n = 120$, a reduction of 0.519. A smaller but parallel decline is observed for the qIT kernel over the same range (0.493 to 0.249). In Scenario B, the highest F1 values are obtained at $Q = 4$, $n = 60$ (RBF: 0.638; qIT: 0.605), indicating that representational compression does not affect both scenarios uniformly.

The variance structure of qIT outputs further characterizes this behavior. The mean standard deviation decreases monotonically with Q: 0.032 at $Q = 2$, 0.023 at $Q = 4$, 0.020 at $Q = 6$, and 0.007 at $Q = 8$. Grouping by n yields no consistent trend (0.022, 0.017, and 0.022 for $n = 60$, 120, and 240, respectively). Encoding resolution is therefore the primary factor governing qIT output variance, rather than training volume [14].

RQ2 — Interaction between n and Q. At a low training volume ($n = 60$), higher F1 values were generally produced by both models in Scenario A than at $n = 120$ or $n = 240$. This behavior suggests that the composition of the nominal training window affects the resulting similarity structure during kernel estimation. Larger training windows may dilute localized transition patterns associated with the

TABLE II

COMPARATIVE F1-SCORE, FALSE ALARM RATE (FAR) AND MISSED ALARM RATE (MAR) RESULTS FOR SCENARIO A AND SCENARIO B ACROSS DIFFERENT QUBIT CONFIGURATIONS AND TRAINING WINDOWS. RBF RESULTS ARE DETERMINISTIC ACROSS SEEDS ($\sigma = 0$). STANDARD DEVIATIONS ARE REPORTED FOR THE QIT KERNEL ($\pm\sigma$, $N = 15$ SEEDS); ENTRIES WITH ± 0.000 INDICATE ZERO VARIANCE ACROSS SEEDS.

Q	n	**Scenario A**						**Scenario B**					
		F1		**FAR**		**MAR**		**F1**		**FAR**		**MAR**	
		RBF	**QIT**	**RBF**	**QIT**	**RBF**	**QIT**	**RBF**	**QIT**	**RBF**	**QIT**	**RBF**	**QIT**
2	60	0.606	0.493 ± 0.019	0.178	0.427 ± 0.031	0.333	0.253 ± 0.045	0.400	0.227 ± 0.060	0.179	0.243 ± 0.027	0.667	0.813 ± 0.055
2	120	0.087	0.249 ± 0.020	0.156	0.292 ± 0.022	0.933	0.733 ± 0.025	0.412	0.226 ± 0.055	0.154	0.101 ± 0.031	0.667	0.848 ± 0.041
2	240	0.176	0.377 ± 0.016	0.356	0.236 ± 0.026	0.800	0.604 ± 0.017	0.160	0.264 ± 0.042	0.051	0.067 ± 0.019	0.905	0.829 ± 0.030
4	60	0.519	0.492 ± 0.017	0.556	0.593 ± 0.023	0.067	0.093 ± 0.042	0.638	0.605 ± 0.017	0.282	0.388 ± 0.009	0.286	0.254 ± 0.029
4	120	0.486	0.385 ± 0.008	0.289	0.507 ± 0.021	0.400	0.400 ± 0.000	0.387	0.230 ± 0.045	0.103	0.128 ± 0.010	0.714	0.838 ± 0.035
4	240	0.400	0.316 ± 0.041	0.467	0.258 ± 0.011	0.400	0.667 ± 0.050	0.541	0.521 ± 0.030	0.154	0.077 ± 0.000	0.524	0.597 ± 0.030
6	60	0.500	0.443 ± 0.013	0.667	0.801 ± 0.006	0.000	0.031 ± 0.034	0.538	0.482 ± 0.013	0.436	0.867 ± 0.011	0.333	0.171 ± 0.030
6	120	0.565	0.439 ± 0.008	0.400	0.616 ± 0.021	0.133	0.200 ± 0.000	0.583	0.313 ± 0.018	0.333	0.503 ± 0.016	0.333	0.641 ± 0.025
6	240	0.429	0.443 ± 0.033	0.889	0.307 ± 0.021	0.000	0.453 ± 0.052	0.571	0.516 ± 0.018	0.231	0.178 ± 0.012	0.429	0.537 ± 0.022
8	60	0.417	0.405 ± 0.000	0.933	0.978 ± 0.000	0.000	0.000 ± 0.000	0.536	0.521 ± 0.011	0.513	0.826 ± 0.014	0.286	0.108 ± 0.022
8	120	0.429	0.371 ± 0.000	0.889	0.933 ± 0.000	0.000	0.133 ± 0.000	0.588	0.302 ± 0.001	0.385	0.614 ± 0.007	0.286	0.619 ± 0.000
8	240	0.429	0.479 ± 0.005	0.889	0.655 ± 0.014	0.000	0.067 ± 0.000	0.549	0.548 ± 0.013	0.410	0.467 ± 0.011	0.333	0.295 ± 0.020

onset of anomalous behavior. A less stable interaction profile is observed in Scenario B. At $Q = 4$, the highest F1 values for both kernels are obtained at $n = 60$. However, at $Q = 8$, the qIT kernel produces a higher F1 value at $n = 240$ than at $n = 60$ (F1 $= 0.548$ vs. 0.521). No uniform advantage is observed for either kernel across all factorial (Q, n) configurations. The response curves therefore indicate that encoding resolution acts as an experimental variable rather than a fixed preprocessing parameter within dc-qml workflows.

V. CONCLUSION

A factorial sensitivity analysis of quantum and classical kernel behavior was presented for industrial anomaly detection under constrained representational conditions. The encoding resolution Q and training volume n were treated as explicit experimental design variables in a data-centric quantum machine learning workflow. Scenarios A and B were evaluated under controlled factorial conditions using RBF and qIT kernels.

The results suggest that kernel behavior varies non-monotonically with the encoding resolution. Larger Q values do not systematically improve F1 Score across the evaluated factorial configurations. In Scenario A, the RBF kernel reached F1 Score of 0.606 at $Q = 2$ and $n = 60$, but decreased to F1 $= 0.087$ at $n = 120$. A smaller reduction was observed for the qIT kernel under the same conditions. These response patterns suggest that representational compression may affect the induced similarity structure during kernel estimation.

Different interaction profiles were also observed between Scenarios A and B due to changes in anomaly ratio and training composition. Larger training windows did not consistently improve detection performance across the evaluated configurations. The factorial response curves suggest that encoding resolution should be treated as an experimental variable rather than a fixed preprocessing parameter within data-centric quantum machine learning workflows.

Future work will include validation on native quantum processors, analysis of temporal tokenization strategies and evaluation under realistic sensor data degradation conditions.

REFERENCES

[1] C. Zhang, D. Song, Y. Chen, X. Feng, C. Lumezanu, W. Cheng, J. Ni, B. Zong, H. Chen, and N. Chawla, "A deep neural network for unsupervised anomaly detection and diagnosis in multivariate time series data," in *AAAI Conference on Artificial Intelligence*, 2018.

[2] S. Badami, "Hardware-agnostic quantum kernel feature mapping for anomaly detection in critical infrastructure: A cross-testbed validation on nisq processors," *IEEE Access*, vol. 14, pp. 49 642–49 654, 2026.

[3] C. Correa-Jullian, S. Cofre-Martel, G. S. Martín, E. L. Droguett, G. de Novaes Pires Leite, and A. B. R. Costa, "Exploring quantum machine learning and feature reduction techniques for wind turbine pitch fault detection," *Energies*, 2022.

[4] S. K. Sheoran, V. Yadav, and R. K. Sheoran, "Robust evaluation of classical and quantum machine learning under noise, imbalance, feature reduction and explainability," *Scientific Reports*, vol. 15, 2025.

[5] A. Ghosh, S. Dutta, A. K. Das, V. K. Shukla, and F. Moreira, "Quantum machine learning in industrial automation," *Quantum Machine Learning in Industrial Automation*, 2025.

[6] M. Ziiatdinov and S. Distefano, "The quantum bottleneck: An analysis of data balancing in qml for security," in *BigHPC@ITADATA*, 2025.

[7] M. R. Pias, E. Flores, B. Guterres, K. D. R. C. Barbosa, and S. da Silva Botelho, "Data-centric quantum machine learning: data-to-models continuum," May 2026, preprint submitted to IEEE Access. [Online]. Available: https://doi.org/10.5281/zenodo.20314756

[8] T. Cultice, M. S. H. Onim, A. Giani, and H. Thapliyal, "Quantum-hybrid support vector machines for anomaly detection in industrial control systems," *ArXiv*, vol. abs/2506.17824, 2025.

[9] K. Tscharke, S. Issel, and P. Debus, "Semisupervised anomaly detection using support vector regression with quantum kernel," *2023 IEEE International Conference on Quantum Computing and Engineering (QCE)*, vol. 01, pp. 611–620, 2023.

[10] A. I. Jawad, E. Stefan-Henningsen, and A. Kiani, "Applications of classical and quantum machine learning in manufacturing: Predictive maintenance, scheduling and tribology," *Next Research*, 2026.

[11] C. Pere, "Data complexity: a threshold between classical and quantum machine learning – part i," 2025.

[12] S. A. C. Ord'onez, L. F. T. Torres, M. Bifulco, C. A. D. Paredes, C. Bosch, and R. S. Carbajo, "Embedding-aware quantum-classical svms for scalable quantum machine learning," in *AIQxQIA@ECAI*, 2025.

[13] M. Kölle, A. Ahouzi, P. Debus, R. Müller, D. Schuman, and C. Linnhoff-Popien, "Towards efficient quantum anomaly detection: One-class svms using variable subsampling and randomized measurements," *arXiv preprint arXiv:2312.09174*, 2023.

[14] M. Kölle, A. Ahouzi, P. Debus, E. Çetiner, R. Müller, D. Schuman, and C. Linnhoff-Popien, "Efficient Quantum One-Class Support Vector Machines for Anomaly Detection Using Randomized Measurements and Variable Subsampling," Jul. 2024.

[15] I. D. Katser and V. O. Kozitsin, "Skoltech anomaly benchmark (skab)," https://www.kaggle.com/dsv/1693952, 2020.